THE JOURNAL OF PHYSICAL CHEMISTRY B

Article

Cite This: J. Phys. Chem. B XXXX, XXX, XXX−XXX

pubs.acs.org/JPCB

Time-Resolved EPR Study of H_2 Reductive Elimination from the Photoexcited Nitrogenase Janus $E_4(4H)$ Intermediate

Published as part of The Journal of Physical Chemistry virtual special issue "David N. Beratan Festschrift".

Dmitriy A. Lukoyanov,[†] Matthew D. Krzyaniak,[†,‡] Dennis R. Dean,[§] Michael R. Wasielewski,[†,‡] Lance C. Seefeldt,*[,∥] and Brian M. Hoffman*[,†]

[†]Department of Chemistry, Northwestern University, Evanston, Illinois 60208, United States

[‡]Institute for Sustainability and Energy at Northwestern, Northwestern University, Evanston, Illinois 60208, United States

[§]Department of Biochemistry, Virginia Polytechnic Institute and State University, Blacksburg, Virginia 24061, United States

[∥]Department of Chemistry and Biochemistry, Utah State University, Logan, Utah 84322, United States

ABSTRACT: Nitrogenase is activated for N_2 reduction through the accumulation of four reducing equivalents at the active-site FeMo-cofactor (FeMo-co: Fe7S9MoC; homocitrate) to form the key Janus intermediate, denoted $E_4(4H)$, whose lowest-energy structure contains two [Fe−H−Fe] bridging hydrides and two protons bound to the sulfurs that also bridge the Fe pairs. In the critical step of catalysis, a H_2 complex transiently produced by reductive elimination (*re*) of the hydrides of $E_4(4H)$, denoted $E_4(H_2;2H)$, undergoes H_2 displacement by N_2, which then undergoes the otherwise energetically unfavorable cleavage of the N≡N triple bond. In pursuing the study of the *re* activation process, we have employed a photochemical approach to obtaining its atomic-level details. Continuous 450 nm irradiation of the ground state of the dihydride Janus intermediate, denoted $E_4(4H)^a$, in an EPR cavity at cryogenic temperatures causes photoinduced *re* of H_2 to generate $E_4(H_2;2H)$. We here extend this photochemical approach with time-resolved EPR studies of the photolysis process on the ns time scale. These studies reveal an additional intermediate in the catalytic reductive elimination process, an isomer of the $E_4(4H)$ FeMo-co metal-ion core that is formed prior to $E_4(H_2;2H)$ and is thought to be created by breaking an Fe−SH bond, thus further integrating the calculational and structural studies into the experimentally determined mechanism by which nitrogenase is activated to cleave the N≡N triple bond.

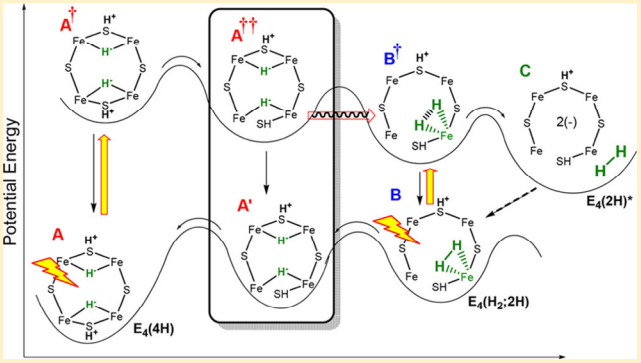

INTRODUCTION

Nitrogenase is activated for N_2 reduction through the accumulation of four reducing equivalents at the active-site FeMo-cofactor (Fe_7S_9MoC; homocitrate) to form the key Janus intermediate, denoted $E_4(4H)$.[1,2] A protocol coupling high-resolution ENDOR measurements to DFT calculations[3] has shown that the lowest-energy structure of this state, Figure 1, contains two [Fe−H−Fe] bridging hydrides and two protons bound to the sulfurs that also bridge the Fe pairs, denoted $E_4(4H)^a$.[4] In the critical step of catalysis (Scheme 1), a H_2 complex transiently produced by reductive elimination (*re*) of the hydrides of $E_4(4H)$, denoted $E_4(H_2;2H)$, undergoes H_2 displacement by N_2, leading to the otherwise energetically unfavorable cleavage of the N≡N triple bond in a thermoneutral process that generates a diazene-level intermediate, denoted the $E_4(2N2H)$ state.[1,4−8] The subsequent delivery of four additional electrons/protons produces two NH_3 products to complete the catalytic cycle.

As a component of these studies, we have pursued a photochemical approach to obtaining atomic-level details of the *re* activation process.[5] Continuous 450 nm irradiation at cryogenic temperatures of the $E_4(4H)^a$ (A in kinetic scheme, Figure 2) in an EPR cavity causes photoinduced reductive

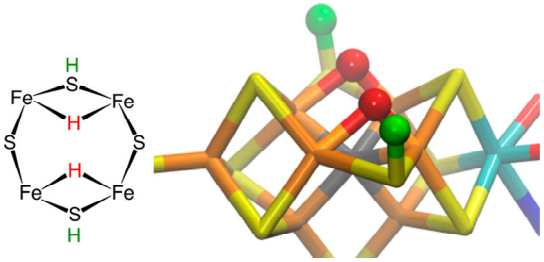

Figure 1. Lowest-energy structure, $E_4(4H)^a$ (ref 4), of the Janus intermediate.

Received: August 14, 2019
Revised: September 19, 2019
Published: September 24, 2019

DOI: 10.1021/acs.jpcb.9b07776
J. Phys. Chem. B XXXX, XXX, XXX−XXX

Scheme 1. Proposed Catalytic Pathway and $E_4(H_2;2H)$ Structure for Activation of the FeMo-Cofactor for N_2 Binding and Reduction

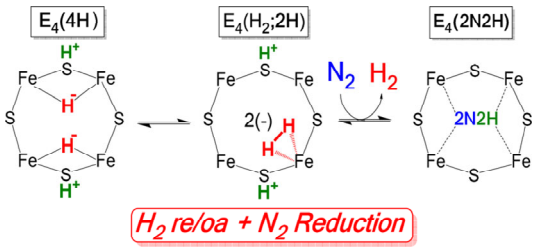

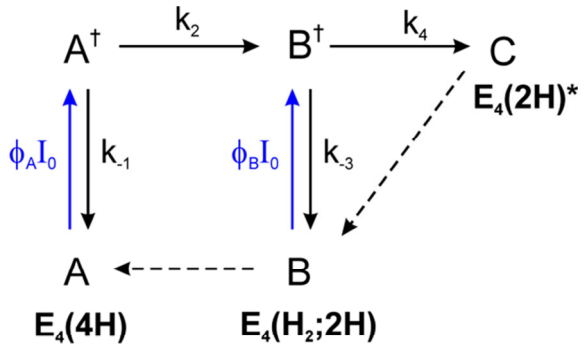

Figure 2. Multistep photolysis scheme proposed for photoinduced conversion $E_4(4H) \rightarrow E_4(2H)^*$ observed in continuous irradiation experiments at $T < 30$ K. Dashed lines represent relaxation pathways that are quenched at cryogenic temperatures.

elimination (*re*) of H_2 to generate the intermediate containing bound H_2, $E_4(H_2;2H)$. The ground-state $E_4(H_2;2H)$ is energetically unable to simply dissociate H_2 unless it is displaced by N_2,[4] but dissociation can occur on the photoexcited energy surface in the frozen matrix, to produce the high-energy doubly reduced intermediate, denoted $E_4(2H)^*$, which corresponds to the state that would form if loss of H_2 could precede N_2 binding.

The low-temperature ($T < 30$ K) photoinduced reductive elimination of the bridging hydrides of $E_4(4H)^a$ was interpreted with the kinetic scheme of Figure 2.[5] In this scheme, the Janus ground state A is excited to state $A^\dagger$ (quantum yield φ_A), which can return to ground (rate constant k_{-1}) or convert by tunneling through an energy barrier to the excited state, $B^\dagger$, of the H_2 complex, B, exhibiting a kinetic isotope effect (KIE) in so doing. The excited state $B^\dagger$ mainly relaxes to B (k_{-3}) but can proceed via loss of H_2 to the final photoproduct state C = [$E_4(2H)^*$ + H_2] ($k_4 < k_{-3}$), where $E_4(2H)^*$ is a high-energy isomer of the $E_2(2H)$ state with the FeMo-co core doubly reduced and two protons reside on sulfurs. This high-energy state is not accessible during catalysis, but when formed photochemically, it is stable to relaxation at $T < 175$ K.[5] The B state, which also is dark-stable at $T < 30$ K, is itself photoactive and can be excited to $B^\dagger$ (quantum yield φ_B). Thus, continuous cycling through this scheme, as occurs during prolonged continuous photolysis, will entirely convert A to C.[5]

In the steady-state experiment, we monitor over minutes the accumulation of the photoproduct state, C, and corresponding loss of Janus state, A. We here report the extension of this photochemical approach to time-resolved EPR studies of the photolysis process on the ns time scale. These reveal an additional intermediate in the reductive elimination process, a "heavy-atom" conformer of $E_4(4H)$ FeMo-co thought to be created by breaking an Fe−SH bond, prior to hydride reductive elimination to generate $E_4(H_2;2H)$.

METHODS

Reagents and General Procedures. All reagents were obtained from Sigma-Aldrich (St. Louis, MO), Fisher Scientific (Fair Lawn, NJ), or Bio-Rad (Hercules, CA) unless specified otherwise and used without further purification. Argon and dinitrogen gases were purchased from Air Liquide America Specialty Gases LLC (Plumsteadville, PA). Manipulation of proteins and buffers was done anaerobically in septum-sealed serum vials and flasks using a vacuum Schlenk line, argon or dinitrogen atmospheres, and gastight syringes. Gas transfers were made using gastight syringes.

Protein Expression and Purification. Nitrogenase proteins (MoFe V70I and Fe protein) were expressed and purified from *Azotobacter vinelandii* strains DJ995 (His-MoFe protein) and DJ884 (Fe protein) as previously described.[9−11]

Sample Preparation. Samples containing the $E_4(4H)$ intermediate in X-band EPR tubes were prepared as described.[5] Attempts to make transparent glassy samples for parallel optical kinetic studies were unsuccessful. The behavior of a nonglass under photolysis has been described.[5]

EPR Kinetic Measurements. Time-resolved EPR (trEPR) measurements were performed at the X-band (~9.5 GHz) using a Bruker Elexsys E680-X/W EPR spectrometer outfitted with a split ring resonator (ER4118X-MS5). The samples were photoexcited at 450 nm with 7 ns, 3 mJ pulses generated by an optical parametric oscillator (Spectra-Physics Basi-scan), pumped with the output of a 10 Hz, frequency-tripled, Nd:YAG laser (Spectra-Physics Quanta-Ray Lab 170). Temperature was maintained at 10 and 5 K using an Oxford Instruments CF935 Cryostat and an ITC503S temperature controller.

The trEPR spectra were collected following photoexcitation, and the kinetic traces of the transient magnetization were acquired in quadrature under continuous wave microwave irradiation (2 mW). The field modulation was disabled to achieve a time response of $Q/\pi\upsilon \approx 17$ ns, where Q is the quality factor of the resonator and υ is the resonant frequency. Kinetic traces were collected at magnetic fields on resonant with the g_1 feature of $E_4(4H)$ and at two field points off-resonance with any transient signals. After every ~4000 spectral acquisitions, the sample tube was moved to provide fresh sample in the active area of the resonator. Each spectrum took approximately 30 min to acquire. In measurements at 10 K, 5 spectra were averaged; in measurements at 5 K, 10 spectra were averaged; both averages were performed following baseline correction, as follows. The EPR spectra were processed in MATLAB. For each kinetic trace, the signal acquired prior to the laser pulse was subtracted from the data and the kinetic traces recorded at magnetic field values off-resonance were considered background signals, whose average was subtracted from the on-resonant kinetic traces. The time traces were fit in Mathcad.

RESULTS AND DISCUSSION

Figure 3 shows the X-band EPR spectrum of $E_4(4H)^a$ before and after continuous irradiation with 450 nm light in the EPR cavity at 12 K, showing the photoconversion from $E_4(4H)^a$ to $E_4(2H)^*$. The $E_4(4H)$ photolysis scheme proposed for $T < 30$

DOI: 10.1021/acs.jpcb.9b07776
J. Phys. Chem. B XXXX, XXX, XXX−XXX

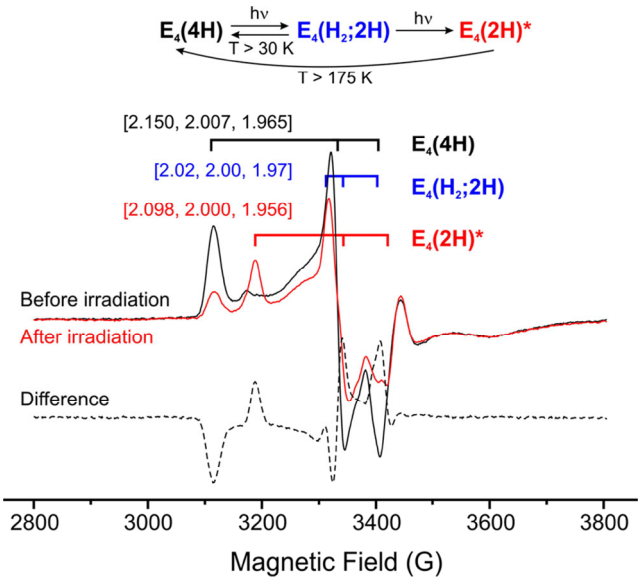

Figure 3. CW EPR spectra of the V70I Ar turnover sample before (black) and after 450 nm continuous irradiation at 12 K (red). Resolved photoinduced spectroscopic changes are explained in accordance with the "two-photon" photolysis scheme shown on top. Irradiation and the spectra acquisition were accomplished as described elsewhere (ref 5).

K continuous irradiation experiments, Figure 2, allows certain predictions for the kinetic behavior of this state as probed in experiments with short (7 ns) laser excitation. Such a laser flash will promptly excite A to state $A^{\dagger}$, which is expected to branch between the rapid return to A (rate constant k_{-1}) and formation of $B^{\dagger}$ (rate constant k_2), which in turn will partition, in part relaxing to B (rate constant k_{-3}) and in part reacting to form C, rate constant k_4. The recovery of A will not be complete because of the conversion to B/C, and the completeness of the recovery is expected to differ for samples in H_2O and D_2O buffer because, as shown in the continuous photolysis experiments, k_2 represents the conversion of bridging hydrides to a bound H_2 and shows a KIE.

To begin this study, progress curves for the EPR signal of the 450 nm laser photoexcited $E_4(4H)^a$ were obtained for H_2O and D_2O samples at g_1 (Figure 4, left). These progress curves show a rapid decrease in intensity upon photoexcitation, followed by slow recovery. The long-time behavior of the traces clearly shows that the recovery process has no solvent kinetic isotope effect. The progress curve is truncated at 15 μs because of limitations introduced by long-time instrumental "drift", and this is not long enough to allow a reliable estimate of the degree to which the recovery of the initial $E_4(4H)^a$ state is incomplete.

Expansion of the initial part of the time course, up to ~600 ns (Figure 4, right), however reveals behavior that is both unexpected, given our observation of photoinduced formation of H_2 during continuous photolysis of $E_4(4H)^a$ ($S = {}^1/_2$), and also quite different from that of the photoexcited FeMo-co resting state (E_0; $S = {}^3/_2$), which relaxes to the ground state within tens of picoseconds.[12] It was anticipated that photolysis of $E_4(4H)^a$ with a 7 ns laser flash would induce a prompt spin-allowed electronic transition to an excited state precursor to H_2 release, whose EPR intensity differs from that of the $E_4(4H)^a$ ground state, and that as a result the 7 ns laser flash would cause a change in the EPR signal that occurs with the instrument response time, ~17 ns. By analogy to the behavior of mononuclear Fe complexes, photon absorption would produce a $S = {}^1/_2$ cluster ligand−metal charge-transfer (LMCT) state, nominally involving electron transfer from S^{2-} to Fe^{3+}, and this would be followed by a sub-ns conversion to a longer-lived "crystal-field" excited state of the Fe ions ($A^{\dagger}$ of Figure 2)[13] that can convert to the excited state of the H_2 complex ($B^{\dagger}$). This interpretation is supported by our recent observation that a photoexcited Fe−S cluster, and FeMo-co is in essence a "Mo-ligated" Fe−S cluster, can act as an electron-transfer donor, presumably from such a crystal-field excited state.[14] However, in the early time portion of the progress curves, Figure 4 (right), it appears that the small change in signal occurs more slowly than the instrument response, and apparently with no solvent kinetic isotope effect; similar behavior is seen at numerous fields across the $E_4(4H)^a$ EPR spectrum. Jointly convolving the two traces with the instrument response yields a time constant for this signal change of ~68 ns.

Subsequent measurements were guided by these observations. To examine the early time behavior in more detail and with better signal/noise, data was collected for a longer time, out only to 3000 ns, and at lower temperature, T = 5 K, in the expectation of slowing the signal response to photolysis, Figure 5. These traces clearly show that the signal decrease is indeed substantially slower than the instrument response time. At this temperature, the response can be well fit to a stretched

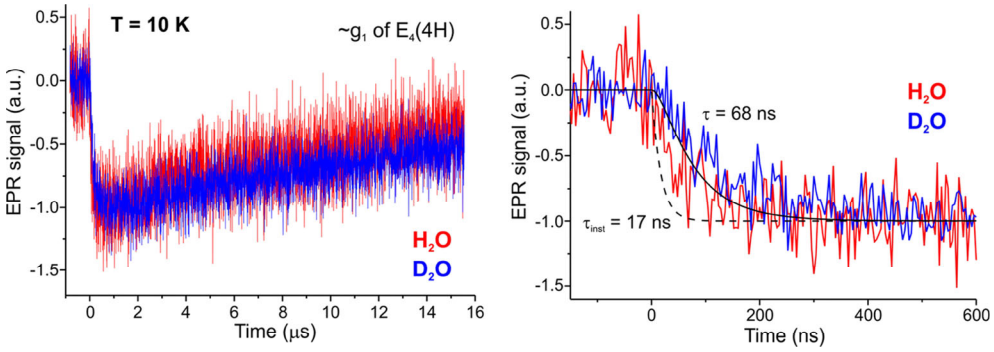

Figure 4. (left) Transient EPR response after 7 ns light pulse excitation of the $E_4(4H)$ state at 10 K (see the Methods). Data were obtained with 4 ns step at magnetic field corresponding to g_1 of $E_4(4H)$ for H_2O (red) and D_2O (blue) samples. (right) Initial part of the time courses shown on the left. The traces of H_2O (red) and D_2O (blue) samples are compared with an exponential decay with the instrument response time (dashed black line; τ_{inst} = 17 ns). Solid line, joint convolution of the two traces with a single exponential function and, τ_{inst}: τ = 68 ns.

DOI: 10.1021/acs.jpcb.9b07776
J. Phys. Chem. B XXXX, XXX, XXX−XXX

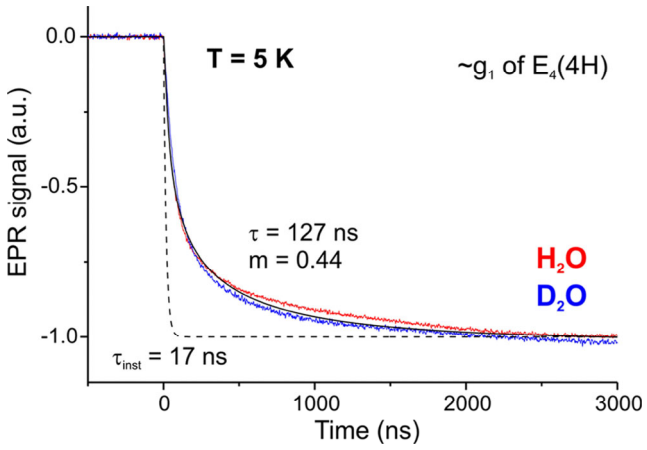

Figure 5. Transient EPR response after 7 ns light pulse excitation of the $E_4(4H)^a$ state at 5 K. Data were obtained with 2 ns step for H_2O (red) and D_2O (blue) samples and normalized to the intensity of the $E_4(4H)^a$ EPR signal. Black traces show the instrument response limit (dashed, τ_{inst} = 17 ns) and fit of the time courses with the stretched exponential function $\exp(-(t/\tau)^m)$ convolved with noninstant instrument response (solid, τ = 127 ns, m = 0.44).

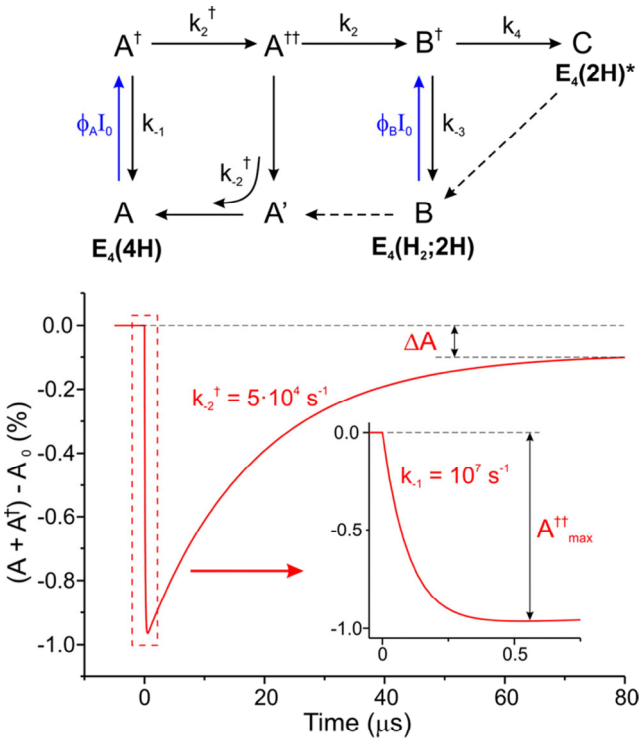

Figure 6. (upper) Photolysis scheme of the photoinduced conversion $E_4(4H) \rightarrow E_4(2H)^*$ modified in accordance with results of short light pulse excitation experiments. Dashed arrows represent relaxation pathways that are quenched at cryogenic temperatures. (lower) Simulation of the experimentally observed transient EPR time course (Figure 4) following laser excitation of $E_4(4H)^a$; initial part shown as an inset. The change of $(A + A^\dagger)$ signal amplitude plotted as the percentage of the photoexcited $A_0 = E_4(4H)^a$ according to the scheme with $k_{-1} = 10^7\ s^{-1}$, $k_2^\dagger = 10^5\ s^{-1}$, $k_{-2}^\dagger = 5 \times 10^4\ s^{-1}$, and $k_2 = 5 \times 10^3\ s^{-1}$.

exponential with a time constant, τ = 127 ns (stretch parameter, m = 0.44; Figure 5, legend), much greater than the instrumental response time ($\tau_{inst} \sim$ 17 ns). In addition, there is clearly no isotope effect on either the decay rate or the extent of the change in signal intensity.

The most likely explanation of this behavior is that within the deadtime of the spectrometer the electronically excited LMCT state indeed relaxes to a ligand-field excited state, $A^\dagger$, that retains the spin-coupling scheme and total $S = {}^1/_2$ of the ground $E_4(4H)^a$ cluster and as a result (surprisingly) retains the ground-state EPR (A) spectrum. Thus, the EPR intensity immediately after photolysis corresponds to the unchanged sum of the signals from A and $A^\dagger$.

The subsequent temporal behavior of the EPR signal, as displayed in the progress curves of Figures 4 and 5, requires that the kinetic scheme of Figure 2 be extended to that of Figure 6, upper, in which the $A^\dagger$ state formed during photoexcitation again can relax to the initial state A, rate constant k_{-1}, but does not convert directly to the H_2-complex excited state, $B^\dagger$. Instead the core of the $A^\dagger$ cluster can isomerize to create a new excited state $A^{\dagger\dagger}$ with rate $k_2^\dagger$.

The reason for the introduction of the more elaborate scheme of Figure 6 is as follows. In the original scheme derived from continuous photolysis, Figure 2, the dihydride state $A^\dagger$ converts directly to the H_2-bound $B^\dagger$ with rate constant k_2 (for that scheme), and the attendant motions of the H's would introduce a KIE in the early time progress curves (Figures 4 and 5), contrary to observation. Instead, the early time change in EPR intensity proceeds with the same extent and the same time constant, τ, in H_2O and D_2O. The absence of an isotope effect shows that this process does not reflect a motion of H^-/H^+ or formation of H_2. Instead, we interpret it as the conversion to a state with an isomerized cluster core, $A^{\dagger\dagger}$, which would be rate-limited by "heavy-atom" (S, Fe) motions that would not introduce an H/D KIE, consistent with experiment.

Both DFT computations[4] and X-ray diffraction studies[15−17] suggest that the photoinduced modification of the $A^\dagger$ cluster core should be interpreted as the cleavage of an [Fe−(SH)−Fe] bond to create a terminal Fe−SH. In the expanded kinetic scheme, the modified $A^{\dagger\dagger}$ conformation of the FeMo-cofactor created by this relatively slow, heavy-atom motion relaxes to the initial state A through recovery of the broken Fe−SH bond. This occurs with an overall rate constant, $k_{-2}^\dagger$, but presumably involves relaxation in two steps, first to the ground state of the $A^{\dagger\dagger}$ conformer, denoted A′, and then its return to the resting A state (Figure 6, upper). The small observed intensity decrease implies this cluster isomerization is much slower than the $A^\dagger$ relaxation, $k_2^\dagger \ll k_{-1}$, and thus only a small population of $A^{\dagger\dagger}$ is generated with a laser flash. Conversely, this analysis supports the DFT-derived structure of $E_4(4H)$ shown in Figure 1, with two bridging hydrides *and* with intact Fe−S bonds for the bridging [Fe−(SH)−Fe] protonated sulfides.

Continuing along the scheme of Figure 6, upper, the $A^{\dagger\dagger}$ state not only relaxes to A but also can undergo follow-up reductive elimination of the bridging hydride(s) to form an excited state of the H_2 complex, $B^\dagger = E_4(H_2;2H)^*$, with a resulting KIE for the rate constant for this process, k_2. In keeping with the continuous photolysis scheme, $B^\dagger$ in turn can either decay to B or proceed to the product seen in continuous photolysis, $C = [E_4(2H)^* + H_2]$ (Figure 6, upper).

Given the temporal "hierarchy" in the progress curves, with the appearance and decay of $A^\dagger$ occurring on the ns time scale but recovery of A on the μs time scale, in addition to the minimal net conversion to B and C, it is straightforward to

DOI: 10.1021/acs.jpcb.9b07776
J. Phys. Chem. B XXXX, XXX, XXX−XXX

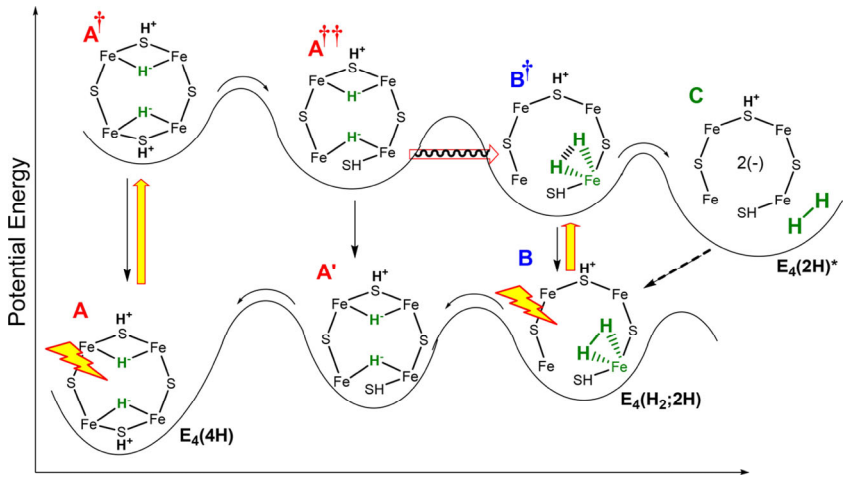

Figure 7. Cartoon representation of the ground- and excited-state potential energy surfaces probed by low-temperature photolysis of the freeze-trapped $E_4(4H)$ intermediate. The red arrow represents the *re* process which introduces a KIE into photolysis and is thought to occur by barrier tunneling. The dashed arrow represents a relaxation process that occurs only at $T \gtrsim 175$ K.

obtain simple formulas from the kinetic scheme of Figure 6, upper, for the maximum population buildup of $A^{\dagger\dagger}$ at the end of the ns decay phase (fraction of the amount of $A^{\dagger}$ created; ${A^{\dagger\dagger}}_{max}$), the time course for this buildup, and, correspondingly, the time course for the early time loss of $A^{\dagger}$

Short-time buildup of $A^{\dagger\dagger}(t)$ and loss of A:

$$\begin{aligned} A^{\dagger\dagger}(t) &\approx {A^{\dagger\dagger}}_{max}(1 - \exp[-(k_{-1} + {k_2}^{\dagger})t]) \\ &\sim {A^{\dagger\dagger}}_{max}(1 - \exp[-(k_{-1})t]) \\ {A^{\dagger\dagger}}_{max} &\approx {k_2}^{\dagger}/(k_{-1} + {k_2}^{\dagger}) \sim {k_2}^{\dagger}/k_{-1} \end{aligned} \quad (1)$$

Likewise, there are simple expressions for the total fractional accumulation of B and C, $(B + C)_{tot}$, which equals the amount of the loss of the initial state, ΔA, and for the time course for the long-time return of the system to the ground state, which is not quite complete because of the partial conversion to B and C

Long-time recovery of A:

$$\begin{aligned} \Delta A &= (B + C)_{tot} \\ &\approx {A^{\dagger\dagger}}_{max}[k_2/({k_{-2}}^{\dagger} + k_2)] \\ &\approx {k_2}^{\dagger}k_2/(k_{-1} + {k_2}^{\dagger})({k_{-2}}^{\dagger} + k_2) \\ &\sim {k_2}^{\dagger}k_2/k_{-1}{k_{-2}}^{\dagger} \sim [{k_2}^{\dagger}/k_{-1}{k_{-2}}^{\dagger}]k_2 \\ &\propto k_2 \end{aligned}$$

$$\begin{aligned} A(t) &\approx (1 - {A^{\dagger\dagger}}_{max}) + ({A^{\dagger\dagger}}_{max} - \Delta A) \\ &\quad \times (1 - \exp[-({k_{-2}}^{\dagger} + k_2)t]) \\ &\rightarrow 1 - \Delta A(\text{long-time}) \end{aligned} \quad (2)$$

The absence of a KIE in the photolysis progress curves, both the early time response to photoexcitation and the long-time recovery, implies that the rate constants, k_{-1}, ${k_2}^{\dagger}$, and ${k_{-2}}^{\dagger}$, have no KIE, and the same for the factor $[{k_2}^{\dagger}/k_{-1}{k_{-2}}^{\dagger}]$. Thus, as discussed above, the finding of KIE ~ 10 for the decay of A during continuous photolysis is directly attributable to an isotope effect on k_2, interpreted as the rate constant for the reductive elimination of the hydrides of $A^{\dagger\dagger}$ to form the bound H_2 of $B^{\dagger}$. This rate constant contributes only to the magnitude of the long-time loss of A, through the parameter ΔA (Figure 6, lower). Unfortunately, this is not measurable here because, as noted above, the extremely slow recovery of the progress curve (Figure 4, left) means the small value of ΔA is not accurately measurable.

Quantitatively connecting these equations to the progress curves for the *early time* loss of EPR intensity as $A^{\dagger\dagger}$ accumulates, the rate constant for this is $k_{-1} \sim 1/\tau_{-1} \sim 10^7$/s ($\tau_{-1} \sim 68$ ns (10 K)/127 ns (5 K)). The loss in EPR intensity through formation of $A^{\dagger\dagger}$ is the product of the fractional accumulation of $A^{\dagger\dagger}$, ${A^{\dagger\dagger}}_{max}$, and the difference in EPR intensities of $A^{\dagger\dagger}$ and $A^{\dagger}$/A. If $A^{\dagger\dagger}$ could be separately examined and that difference were thus known, we could derive the value of ${k_2}^{\dagger}/k_{-1}$ and thus of ${k_2}^{\dagger}$ from the short-time change in intensity, but this is not the case. However, if we take as a limiting value that $A^{\dagger\dagger}$ has no detectable EPR signal at this field and estimate the fractional change in signal to be $(\Delta I/I_0) \sim 1\%$, then an *upper bound* to ${k_2}^{\dagger}$ can be estimated from the measured maximum short-time change in intensity: ${k_2}^{\dagger} \leq (\Delta I/I_0)k_{-1} \lesssim 0.01k_{-1} \sim 10^5$/s between 5 and 10 K. The rate constant for the *long-term relaxation* to the ground state, A, is given by ${k_{-2}}^{\dagger} \approx 1/{\tau_{-2}}^{\dagger} \sim 1/17\ \mu s \sim 5 \times 10^4$/s. The only rate constant that exhibits a KIE is k_2, so ΔA should also show an isotope effect. Because the long-time traces (Figure 4, left) show no clear KIE, this requires ΔA and thus k_2 to be very small, $k_2 \lesssim {k_{-2}}^{\dagger}/10 \sim 10^3$–$10^4$ s^{-1}. One can further partition the sum $(B + C)_{tot}$ into the fractional accumulations of the individual products of photolysis, B and C,

$$\begin{aligned} B_{tot} &\approx (B + C)_{tot}[k_{-3}/(k_{-3} + k_4)] \propto k_2[k_{-3}/(k_{-3} + k_4)] \\ C_{tot} &\approx (B + C)_{tot}[k_4/(k_{-3} + k_4)] \propto k_2[k_4/(k_{-3} + k_4)] \end{aligned} \quad (3)$$

As one might expect that both k_{-3} and k_4 will have a KIE, the individual accumulations of B and C will in general exhibit KIEs different from each other and different from that of their sum.

CONCLUSIONS

We have captured the time-resolved kinetic progress curves obtained upon ns photolysis of the ground state of the $E_4(4H)$

DOI: 10.1021/acs.jpcb.9b07776
J. Phys. Chem. B XXXX, XXX, XXX–XXX

Janus intermediate, Figure 1. This state, denoted A in the kinetic schemes of Figures 6 and 7, carries four reducing equivalents stored as [Fe−H−Fe] hydrides bridging Fe2/Fe6 and Fe3/Fe7, and two protons bound to the sulfides that also bridge those Fe pairs.[3] In the kinetic scheme that describes the progress curves, Figure 6, upper, the photoexcited A state, denoted $A^{\dagger}$, can relax or undergo a conformational change without a KIE, indicating that this change is rate-limited by "heavy-atom" motions of the FeMo-co core. The precise structure of $A^{\dagger\dagger}$ is of course not revealed by the present study. However, as discussed above, we propose that, as visualized in Figure 7, $A^{\dagger\dagger}$ is the excited state of an $E_4(4H)^a$ conformer (A′) having undergone cleavage of an Fe−SH bond. The lability of this bond is suggested by recent X-ray and DFT studies. The excited state $A^{\dagger\dagger}$ can relax to its ground state A′, and hence to A, but can also undergo *re* of the two hydrides to form the excited H_2-bound state, $B^{\dagger}$, Figure 7. The interpretation of this step, with its change in bonds to H's, is supported by the observation that its rate constant in the kinetic scheme of Figure 6, upper, k_2, must exhibit the KIE seen in continuous photolysis experiments. $B^{\dagger}$ can then relax to B (which itself is photoactive) or proceed to release H_2 in these experiments, creating the otherwise inaccessible, high-energy state C = [$E_4(2H)^*$ + H_2], involving a high-energy conformer of the hydride-bound $E_2(2H)$ state.[4]

Focusing on the ground-state surface thus implied by the present study, Figure 7, the photophysical approach has yielded new experimental insights into the catalytic reductive elimination process undergone by the Janus $E_4(4H)$ intermediate. By resolving a kinetic intermediate, it reveals the presence of a "heavy-atom" isomer of $E_4(4H)$ FeMo-co thought to be created by breaking an Fe−SH bond, supporting the idea of the hemilability of such a bond and thus further integrating the calculational and structural studies into the experimentally determined mechanism by which nitrogenase is activated to cleave the N≡N triple bond.

AUTHOR INFORMATION

Corresponding Authors

*E-mail: lance.seefeldt@usu.edu. Phone: +1.435.797.3964.
*E-mail: bmh@northwestern.edu. Phone: +1.847.491.3104.

ORCID

Matthew D. Krzyaniak: 0000-0002-8761-7323
Michael R. Wasielewski: 0000-0003-2920-5440
Lance C. Seefeldt: 0000-0002-6457-9504
Brian M. Hoffman: 0000-0002-3100-0746

Notes

The authors declare no competing financial interest.

ACKNOWLEDGMENTS

This work was supported by the NSF (MCB 1908582, B.M.H.; CHE-1900422, M.R.W.), and the preparation of protein samples was supported by a grant from the U.S. Department of Energy, Office of Science, Basic Energy Sciences (BES) under awards to L.C.S. and D.R.D. (DE-SC0010687 and DESC0010834).

REFERENCES

(1) Hoffman, B. M.; Lukoyanov, D.; Yang, Z. Y.; Dean, D. R.; Seefeldt, L. C. Mechanism of Nitrogen Fixation by Nitrogenase: The Next Stage. *Chem. Rev.* **2014**, *114*, 4041−4062.

(2) Harris, D. F.; Lukoyanov, D. A.; Kallas, H.; Trncik, C.; Yang, Z.-Y.; Compton, P.; Kelleher, N.; Einsle, O.; Dean, D. R.; Hoffman, B. M.; Seefeldt, L. C. Mo-, V-, and Fe-Nitrogenases Use a Universal Eight-Electron Reductive-Elimination Mechanism to Achieve N_2 Reduction. *Biochemistry* **2019**, *58*, 3293−3301.

(3) Hoeke, V.; Tociu, L.; Case, D. A.; Seefeldt, L. C.; Raugei, S.; Hoffman, B. M. High-Resolution Endor Spectroscopy Combined with Quantum Chemical Calculations Reveals the Structure of Nitrogenase Janus Intermediate $E_4(4H)$. *J. Am. Chem. Soc.* **2019**, *141*, 11984−11996.

(4) Raugei, S.; Seefeldt, L. C.; Hoffman, B. M. A Critical Computational Analysis Illuminates the Reductive-Elimination Mechanism that Activates Nitrogenase for N_2 Reduction. *Proc. Natl. Acad. Sci. U. S. A.* **2018**, *115*, E10521−E10530.

(5) Lukoyanov, D.; Khadka, N.; Dean, D. R.; Raugei, S.; Seefeldt, L. C.; Hoffman, B. M. Photoinduced Reductive Elimination of H_2 from the Nitrogenase Dihydride(Janus) State Involves a FeMo-Cofactor-H_2 Intermediate. *Inorg. Chem.* **2017**, *56*, 2233−2240.

(6) Lukoyanov, D.; Khadka, N.; Yang, Z. Y.; Dean, D. R.; Seefeldt, L. C.; Hoffman, B. M. Reductive Elimination of H_2 Activates Nitrogenase to Reduce the N≡N Triple Bond: Characterization of the $E_4(4H)$ Janus Intermediate in Wild-Type Enzyme. *J. Am. Chem. Soc.* **2016**, *138*, 10674−10683.

(7) Lukoyanov, D.; Khadka, N.; Yang, Z. Y.; Dean, D. R.; Seefeldt, L. C.; Hoffman, B. M. Reversible Photoinduced Reductive Elimination of H_2 from the Nitrogenase Dihydride State, the $E_4(4H)$ Janus Intermediate. *J. Am. Chem. Soc.* **2016**, *138*, 1320−1327.

(8) Lukoyanov, D.; Yang, Z. Y.; Khadka, N.; Dean, D. R.; Seefeldt, L. C.; Hoffman, B. M. Identification of a Key Catalytic Intermediate Demonstrates That Nitrogenase Is Activated by the Reversible Exchange of N_2 for H_2. *J. Am. Chem. Soc.* **2015**, *137*, 3610−3615.

(9) Christiansen, J.; Goodwin, P. J.; Lanzilotta, W. N.; Seefeldt, L. C.; Dean, D. R. Catalytic and Biophysical Properties of a Nitrogenase Apo-MoFe Protein Produced by a *Nifb*-Deletion Mutant of *Azotobacter Vinelandii*. *Biochemistry* **1998**, *37*, 12611−12623.

(10) Burgess, B. K.; Jacobs, D. B.; Stiefel, E. I. Large-Scale Purification of High Activity *Azotobacter Vinelandii* Nitrogenase. *Biochim. Biophys. Acta* **1980**, *614*, 196−209.

(11) Peters, J. W.; Fisher, K.; Dean, D. R. Identification of a Nitrogenase Protein-Protein Interaction Site Defined by Residues 59 through 67 within the *Azotobacter Vinelandii* Fe Protein. *J. Biol. Chem.* **1994**, *269*, 28076−28083.

(12) Mao, Z.; Liou, S.-H.; Khadka, N.; Jenney, F. E.; Goodin, D. B.; Seefeldt, L. C.; Adams, M. W. W.; Cramer, S. P.; Larsen, D. S. Cluster-Dependent Charge-Transfer Dynamics in Iron−Sulfur Proteins. *Biochemistry* **2018**, *57*, 978−990.

(13) McCusker, J. K. Electronic Structure in the Transition Metal Block and Its Implications for Light Harvesting. *Science* **2019**, *363*, 484−488.

(14) Yang, H.; McDaniel, E. C.; Impano, S.; Byer, A. S.; Jodts, R. J.; Yokoyama, K.; Broderick, W. E.; Broderick, J. B.; Hoffman, B. M. The Elusive 5′-Deoxyadenosyl Radical: Captured and Characterized by Electron Paramagnetic Resonance and Electron Nuclear Double Resonance Spectroscopies. *J. Am. Chem. Soc.* **2019**, *141*, 12139−12146.

(15) Spatzal, T.; Perez, K. A.; Einsle, O.; Howard, J. B.; Rees, D. C. Ligand Binding to the FeMo-cofactor: Structures of CO-bound and reactivated nitrogenase. *Science* **2014**, *345*, 1620−1623.

(16) Sippel, D.; Rohde, M.; Netzer, J.; Trncik, C.; Gies, J.; Grunau, K.; Djurdjevic, I.; Decamps, L.; Andrade, S. L. A.; Einsle, O. A Bound Reaction Intermediate Sheds Light on the Mechanism of Nitrogenase. *Science* **2018**, *359*, 1484−1489.

(17) Sippel, D.; Einsle, O. The Structure of Vanadium Nitrogenase Reveals an Unusual Bridging Ligand. *Nat. Chem. Biol.* **2017**, *13*, 956−960.

DOI: 10.1021/acs.jpcb.9b07776
J. Phys. Chem. B XXXX, XXX, XXX−XXX